

**SYNTHESIS, CHARACTERIZATION AND APPLICATION OF SILVER
ALLIED NANOBIMETALLIC PARTICLES FOR CATALYSIS**

BY

ADEKOYA, JOSEPH ADEYEMI

(CUGP07186)

**DEPARTMENT OF CHEMISTRY
SCHOOL OF NATURAL AND APPLIED SCIENCES
COLLEGE OF SCIENCE AND TECHNOLOGY
COVENANT UNIVERSITY, OTA**

MARCH, 2014

**SYNTHESIS, CHARACTERIZATION AND APPLICATION OF SILVER ALLIED
NANOBIMETALLIC PARTICLES FOR CATALYSIS**

BY

ADEKOYA, JOSEPH ADEYEMI (CUGP07186)

**HND (SLT Chemistry) Ogun Poly; PGD (Analytical/Environmental Chemistry) LASU; M.Sc
(Analytical/Environmental Chemistry) LASU**

**A THESIS SUBMITTED TO THE POSTGRADUATE SCHOOL OF COVENANT
UNIVERSITY, OTA, OGUN STATE, NIGERIA**

**IN PARTIAL FULFILMENT OF THE REQUIREMENTS FOR THE AWARD OF
DOCTOR OF PHILOSOPHY (Ph.D) DEGREE IN CHEMISTRY, IN THE
DEPARTMENT OF CHEMISTRY, SCHOOL OF NATURAL & APPLIED
SCIENCES, COLLEGE OF SCIENCE & TECHNOLOGY, COVENANT
UNIVERSITY, OTA**

MARCH, 2014

DECLARATION

I, **ADEKOYA, Joseph Adeyemi**, hereby declare that this thesis is a product of my own unaided research work. It has not been submitted, either wholly or in part to this or any other institution for the award of any degree, diploma or certificate. All sources of scholarly information that were used in this thesis were duly acknowledged.

.....

ADEKOYA, Joseph Adeyemi

CERTIFICATION

We certify that the thesis titled “Synthesis, Characterization and Application of Silver Allied Nanobimetallic Particles for Catalysis” is an original work carried out by Mr. Joseph Adeyemi Adekoya (CUGP07186) in the Department of Chemistry, Covenant University, Ota, Ogun state under the supervision of Dr. Enock O. Dare and Prof. M. Adediran Mesubi. We have examined and found the work acceptable for the award of a degree of Doctor of Philosophy in Chemistry.

Dr. Enock O. Dare

(Supervisor)

Department of Chemistry,

Federal University of Agriculture, Abeokuta.

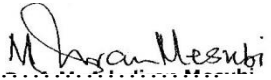
Signature/Date 

Prof. M. Adediran Mesubi

(Co-Supervisor)

Department of Chemistry,

Covenant University, Ota.

Signature/Date 

Dr. K. O. Ajanaku

(HOD Chemistry)

Department of Chemistry,

Covenant University, Ota.

Signature/Date

Prof. R. A. Oderinde

(External Examiner)

University of Ibadan, Ibadan.

Signature/Date

Prof. C. A. Loto

Dean, College of Science and Technology,

Covenant University, Ota.

Signature/Date

DEDICATION

This thesis is dedicated to the Almighty God, my creator, provider and wisdom. To Him alone be all the glory.

ACKNOWLEDGEMENTS

I give glory to God the source of all wisdom and knowledge for the successful completion of this work. I am greatly indebted to the Chancellor and the Chairman of the Board of Regents, Covenant University, Canaanland, Ota, Dr. David Oyedepo for giving me the opportunity to pursue an academic career which I cherish very much.

I am full of gratitude to my Supervisor, Dr. Enock O. Dare and my Co-supervisor, Prof. M. Adediran Mesubi for the research idea, constructive criticism and their guidance all through the work. The corrections and contribution of the panel of examiners: Prof. R. A. Oderinde (external examiner) of Department of Chemistry, University of Ibadan, Ibadan; Prof. J. A. Omoleye of Department of Chemical Engineering; Drs. K. O. Ajanaku (Chief Examiner) and A. I. Inegbenedor of Department of Chemistry; Dr. M. Egharevba, representative of School of Postgraduate Studies, Covenant University, Ota is greatly acknowledged. Likewise, the inestimable contribution and correction of my external assessors: Prof. I. C. Eromosele of Chemistry Department, Federal University of Agriculture, Abeokuta and Prof. A. Y. Fasasi of Centre for Energy Research and Development, Obafemi Awolowo University, Ile-Ife is highly appreciated. The effort and contribution of my internal assessor, Dr. O. O. Ajayi of Department of Mechanical Engineering, Covenant University, Ota is also acknowledged. My sincere appreciation goes to Prof. A. A. Adeniyi of Chemistry Department, Lagos State University, Ojo for investing his time and resources to secure the collaboration that enabled me to complete this work. I am thankful to Prof. K. O. Okonjo, for his encouragement and support, as well as for his invaluable advice in treating the kinetic data of this work. My gratitude also goes to the following: the Dean/Deputy Dean School of Postgraduate Studies, Prof. Charles Ogbulogo and Dr. A. Daramola respectively, the Dean, College of Science and Technology, Prof. C. A. Loto, the Deputy Dean, School of Natural and Applied Sciences, Dr. O. O. Obembe. I greatly appreciate their moral support and encouragement. I am very grateful to both the past and present HODs of Chemistry Department namely, Professors M. Adediran Mesubi and JohnBull O. Echeme, Drs. A. I. Inegbenedor and K. O. Ajanaku for their strong support and interest in my career.

I am greatly indebted to Prof. Neerish Revaprasadu of University of Zululand, KwaDlangezwa, South Africa for the collaboration, without which it would not have been possible for me to complete this work. My gratitude also goes to the following: Late Dr. Adeola Nejo, Babcock University, Ilisan Remo, Ogun State, for the contact he provided and the Transmission Electron Microscope (TEM) analysis, Sixbirth A. Mlowe, a friend that

made my settling to work in South Africa easy and also for helping with TEM analysis; Drs Funke Nejo, R. Segapelo, N. Rajasekhar and D. Musa; Messrs Welcome Zibane, Joseph Kyobe and N. Mxolisi for their help and encouragement while working together in South Africa.

The friendship and encouragement from my colleagues in the Department is highly appreciated. I deeply appreciate my lovely wife and jewel, Mrs. Dorcas Omobosedede Adekoya and my dearest children: David Tirenoluwa Adekoya, Faith Iyanuoluwa Adekoya and Favour Oreoluwa Adekoya for their moral support and understanding especially at a time when I travelled to South Africa for the bench work. I am fond of you all. I also deeply appreciate my lovely parents, Reverend Samuel Adekoya and Deaconess Felicia Adekoya for their support and prayers. My siblings, relations and the entire pastorate of the Christian Assembly Mission are hereby acknowledged with gratitude and appreciation.

Adekoya, Joseph Adeyemi

TABLE OF CONTENTS

| Contents | Pages |
|------------------------------------|--------------|
| Title Page | i |
| Declaration | iii |
| Certification | iv |
| Dedication | v |
| Acknowledgements | vi |
| Table of Contents | viii |
| List of Tables | xiii |
| List of Figures | xv |
| List of Acronyms and Abbreviations | xxiv |
| Abstract | xxvi |

CHAPTER ONE

1.0 INTRODUCTION

| | |
|---|----|
| 1.1 Background of the Study | 1 |
| 1.2 Crystalline Solids and their Periodicity | 2 |
| 1.2.1 Bloch's Theorem | 3 |
| 1.3 Morphological Properties of Metals | 4 |
| 1.4 Electronic Structure and Optical Properties of Metals | 5 |
| 1.4.1 Electronic Conduction | 6 |
| 1.5 The Effects of the Nanometer Length Scale | 8 |
| 1.5.1 Changes in the Total Energy of the System | 9 |
| 1.5.2 Changes in the System Structure | 10 |
| 1.5.2.1 Vacancies in Nanocrystals | 11 |
| 1.5.2.2 Dislocation in Nanocrystal | 12 |
| 1.5.3 Effect of nanoscale dimensions on the properties of nanomaterials | 14 |
| 1.5.3.1 Effect on Structural Properties | 14 |
| 1.5.3.2 Effect on Thermal Properties | 16 |
| 1.5.3.3 Effect on Chemical Properties | 17 |
| 1.5.3.4 Effect on Mechanical Properties | 17 |
| 1.5.3.5 Magnetic Properties | 18 |
| 1.5.3.6 Optical Properties | 19 |

| | |
|--------------------------------|----|
| 1.5.3.7 Electronic Properties | 19 |
| 1.6 Aim of the Study | 20 |
| 1.7 Objectives of the Study | 20 |
| 1.8 Justification of the Study | 21 |
| 1.9 Statement of Problem | 22 |

CHAPTER TWO

2.0 LITERATURE REVIEW

| | |
|---|----|
| 2.1 Classification of Nanostructures | 23 |
| 2.2 Colloidal Metal Nanoparticles | 25 |
| 2.3 Bimetallic Nanoparticles | 27 |
| 2.3.1 The Influence of Bimetallic Nanoparticles on Improving Plasmonic Properties | 29 |
| 2.4 Methods of Preparation of Bimetallic Nanomaterials | 31 |
| 2.4.1 Top-Down Approach | 32 |
| 2.4.2 Bottom-Up Approach | 32 |
| 2.4.2.1 Vapour Phase Deposition method | 32 |
| 2.4.2.2 Plasma-Assisted Deposition Process | 34 |
| 2.4.2.3 Molecular Beam Epitaxy and Metal-organic Vapour Phase Epitaxy | 36 |
| 2.4.2.4 Sol-gel Methods | 36 |
| 2.4.2.5 Colloidal Methods | 38 |
| 2.4.2.6 Co-precipitation Synthetic Method | 38 |
| 2.5 Theory and Thermodynamics of Co-precipitation | 39 |
| 2.5.1 Nucleation | 41 |
| 2.5.2 Growth | 42 |
| 2.5.3 Oswald Ripening | 42 |
| 2.5.4 Growth Termination and Nanoparticle Stabilization | 43 |
| 2.5.5 Purification of Colloidal Metal Nanoparticles | 45 |
| 2.6 Characterization of Bimetallic Nanoparticles | 46 |
| 2.6.1 Spectroscopy Techniques for Bimetallic Nanoparticles | 46 |
| 2.6.2 Transmission Electron Microscopy | 47 |
| 2.6.3 X-ray Diffraction | 48 |
| 2.6.4 X-Ray Photoelectron Spectroscopy (XPS) | 48 |

| | | |
|---------|---|----|
| 2.6.5 | Optical Measurements | 49 |
| 2.6.5.1 | UV/Vis Spectroscopy | 50 |
| 2.6.5.2 | Photoluminescence | 51 |
| 2.7 | Polymer and Ligand Stabilized Silver Based Bimetallic Nanoparticles | 54 |
| 2.7.1 | AgCo Bimetallic System | 56 |
| 2.7.2 | AgNi Bimetallic System | 57 |
| 2.7.3 | AgPt Bimetallic System | 58 |
| 2.7.4 | AgPd Bimetallic System | 60 |
| 2.7.5 | AgRu Bimetallic System | 62 |
| 2.8 | Application of Metallic Nanoparticles | 62 |
| 2.8.1 | Therapeutic in Vivo Applications | 63 |
| 2.8.2 | Diagnostic in Vitro Applications | 65 |
| 2.8.3 | Future Applications of Magnetic Nanoparticles | 66 |

CHAPTER THREE

3.0 MATERIALS AND METHODS

| | | |
|------|---|----|
| 3.1 | Chemicals and Reagents | 67 |
| 3.2 | Synthesis of Ag Nanoparticles in Polyols, Trisodium citrate, TOPO and HDA | 67 |
| 3.3 | Synthesis of Bimetallic AgCo Nanoparticles in Polyols | 69 |
| 3.4 | Synthesis of Bimetallic AgNi Nanoparticles in Polyols | 70 |
| 3.5 | Synthesis of Bimetallic AgPd Nanoparticles in Polyols | 71 |
| 3.6 | Synthesis of Bimetallic AgPt Nanoparticles in Polyols | 72 |
| 3.7 | Synthesis of Bimetallic AgRu Nanoparticles in Dodecanethiol | 73 |
| 3.8 | Aqueous Synthesis of Silver Allied Bimetallic Nanoparticles Using Pentaerythritol and Trisodium citrate as Capping Agent and Surfactant | 73 |
| 3.9 | Synthesis of Organically Capped AgM Allied Bimetallic Nanoparticles Using TOPO and HDA as Capping Agents | 74 |
| 3.10 | Synthesis of Monometallic Co, Ni, Pd, Pt and Ru Nanoparticles in Polyols, Dodecanethiol and Trisodium citrate | 75 |
| 3.11 | Characterization | 76 |
| 3.12 | Kinetics of Catalytic Reduction of p-nitrophenol in the Presence of NaBH ₄ Solution Using the Prepared AgPd and AgPt Nanoparticles | 77 |

CHAPTER FOUR

4.0 RESULTS AND DISCUSSION

| | | |
|-------|--|-----|
| 4.1 | Optical (UV/Vis and PL) Spectra of Ag Nanoparticles in Polyols, SC, TOPO and HDA | 78 |
| 4.1.1 | TEM and HRTEM Results of Ag Nanoparticles Stabilized with EG, GLY, SC and PET | 83 |
| 4.1.2 | XRD Patterns of Ag Nanoparticles Stabilized with EG, DEG, GLY, SC and PET | 86 |
| 4.2 | Optical (UV/Vis and PL) Spectra of AgCo Nanoparticles in Polyols | 87 |
| 4.2.1 | TEM and HRTEM Results of AgCo Nanoparticles in Polyols | 91 |
| 4.2.2 | XRD Patterns AgCo Nanoparticles in Polyols | 93 |
| 4.2.3 | XPS Result of AgCo in Polyol | 94 |
| 4.3 | Optical (UV/Vis and PL) Spectra of AgNi Nanoparticles in Polyols | 97 |
| 4.3.1 | TEM and HRTEM Results of AgNi Nanoparticles in Polyols | 101 |
| 4.3.2 | XRD Patterns AgCo Nanoparticles in Polyols | 104 |
| 4.3.3 | XPS Result of AgNi in Polyols | 105 |
| 4.4 | Optical (UV/Vis and PL) Spectra of AgPd Nanoparticles in Polyols | 108 |
| 4.4.1 | TEM and HRTEM Results of Ag/Pd Nanoparticles in Polyols | 113 |
| 4.4.2 | XRD Patterns of Ag/Pd in Polyols | 115 |
| 4.4.3 | XPS Result for Ag/Pd in Polyols | 117 |
| 4.5 | Optical Properties of Bimetallic AgPt Synthesized in Polyols | 119 |
| 4.5.1 | TEM and HRTEM Results of Ag/Pt Nanoparticles in Polyols | 125 |
| 4.5.2 | X-ray Diffraction Result of AgPt in Polyols | 129 |
| 4.5.3 | XPS Result of AgPt in Polyols | 130 |
| 4.6 | Optical Properties of AgRu Nanoparticles in Dodecanethiol | 133 |
| 4.6.1 | TEM and HRTEM Images of AgRu nanoparticles in Dodecanethiol | 137 |
| 4.6.2 | XRD Pattern of AgRu Nanoparticles in Dodecanethiol | 140 |
| 4.7 | Optical Properties of Ag Allied Bimetallic Nanoparticles Capped with Pentaerythritol and Trisodium citrate | 141 |
| 4.7.1 | TEM and HRTEM Images of Ag Allied Bimetallic Nanoparticles Capped with Pentaerythritol and Trisodium citrate | 146 |
| 4.7.2 | XRD Patterns of Ag Allied Bimetallic Nanoparticles Capped with Pentaerythritol and Trisodium citrate | 152 |

| | | |
|-------------------------|--|-----|
| 4.7.3 | XPS Result of AgRu Bimetallic Nanoparticles Capped with Pentaerythritol | 154 |
| 4.8 | Optical Properties of Organically Capped Ag Allied Bimetallic Nanoparticles Using HDA and TOPO as Capping Agents | 156 |
| 4.8.1 | TEM and HRTEM Images of Organically Capped Ag Allied Bimetallic Nanoparticles Using HDA and TOPO as Coordinating Ligands | 162 |
| 4.8.2 | XRD Results of Organically Capped Ag Allied Bimetallic Nanoparticles | 168 |
| 4.8.3 | XPS Results of Organically Capped AgRu Allied Bimetallic Nanoparticles Using TOPO as Capping Agent | 169 |
| 4.9 | Formation Mechanism of Bimetallic Core-Shell Nanoparticles | 172 |
| 4.10 | TEM Images of Some Monometallic Nanoparticles | 174 |
| 4.10.1 | XRD Patterns of Some Monometallic Nanoparticles | 177 |
| 4.11 | Results of Catalysis Studies | 180 |
| CHAPTER FIVE | | |
| 5.0 | CONCLUSION AND RECOMMENDATIONS | |
| 5.1 | Conclusion | 195 |
| 5.2 | Recommendations | 197 |
| 5.3 | Contributions to knowledge | 198 |
| | REFERENCES | 199 |
| | Appendices | 226 |

LIST OF TABLES

| | | Pages |
|------------|--|-------|
| Table 2.1 | Examples of Reduced Dimensionality Systems | 25 |
| Table 2.2 | Classification of Optical Spectroscopy Methods | 52 |
| Table 4.1 | Summary of the Physical Parameters of Ag Nanoparticles Synthesized in Polyols, SC, TOPO and HDA | 82 |
| Table 4.2 | Summary of the Physical Parameters of Bimetallic AgCo Nanoparticles Synthesized in Polyols | 90 |
| Table 4.3 | Summary of the Physical Parameters of Bimetallic AgNi Nanoparticles Synthesized in Polyols | 100 |
| Table 4.4 | Summary of the Physical Parameters of Bimetallic AgPd Nanoparticles Synthesized in Polyols | 109 |
| Table 4.5 | Summary of the Physical Parameters of Bimetallic AgPt Nanoparticles Synthesized in Polyols | 121 |
| Table 4.6 | Summary of the Physical parameters of Bimetallic AgRu Nanoparticles Synthesized in Dodecanethiol | 134 |
| Table 4.7 | Summary of the Physical Parameters of Ag Allied Bimetallic Nanoparticles Using Pentaerythritol as Capping Agent | 143 |
| Table 4.8 | Summary of the Physical Parameters of Ag Allied Bimetallic Nanoparticles Using Trisodium Citrate as Surfactant | 144 |
| Table 4.9 | Summary of the Physical Parameters of Synthesized Organically Capped Ag Allied Bimetallic Nanoparticles Using TOPO and HDA as Capping Agents | 158 |
| Table 4.10 | Summary of the Physical Parameters of Synthesised Monometallic Co, Ni, Pd, Pt and Ru Nanoparticles in Polyols | 179 |
| Table 4.11 | Summary of the Physical Parameters of Synthesised Monometallic Co, Ni, Pd, Pt and Ru Nanoparticles in PET, SC and DT | 179 |
| Table 4.12 | Summary of the Data for Catalytic Reduction of p-nitrophenol in the Presence of NaBH ₄ Solution Using Some of the Prepared AgPt Nanoparticles | 182 |
| Table 4.13 | Summary of the data for Catalytic Reduction of p-nitrophenol in the Presence of NaBH ₄ Solution Using Some of the Prepared AgPd Nanoparticles | 183 |

| | | |
|------------|--|-----|
| Table 4.14 | Summary of the Data for Catalytic Reduction of p-nitrophenol in the Presence of NaBH ₄ Solution Using Some of the Prepared AgPt Nanoparticles | 184 |
| Table 4.15 | Summary of Observed Rate Constant of Ag allied Nanobimetallic Particles | 192 |

LIST OF FIGURES

| | | Pages |
|-------------|--|-------|
| Figure 1.1 | Electronic Densities of States for Semiconductor Nanostructures of Various Dimensions | 6 |
| Figure 1.2 | (a) Electron Energy Band Gap Structure Diagram and (b) Density of States for Crystalline $\text{Ag}_2\text{ZnGeO}_4$ | 7 |
| Figure 1.3 | SEM Images of Noble Metal Nanocrystals | 15 |
| Figure 1.4 | Computed Value of the Average Magnetic Moment of Ni Clusters at $T=200$ K for Various Cluster Sizes (50-700 atoms) | 18 |
| Figure 2.1 | Classification of Nanostructures with Different Dimensionalities | 23 |
| Figure 2.2 | Morphology of Bimetallic Nanoparticles | 30 |
| Figure 2.3 | Aerosol Assisted Chemical Vapour Deposition System | 33 |
| Figure 2.4 | DC glow discharge Apparatus | 35 |
| Figure 2.5 | Magnetron Sputtering Apparatus | 35 |
| Figure 2.6 | Molecular Structures of Some Organic Stabilizers | 44 |
| Figure 2.7 | Molecular Structures of Some Organic Stabilizers/Coordinating Ligands | 45 |
| Figure 2.8 | Jablonski diagram for one-photon (a) and two-photon (b) excitation | 53 |
| Figure 2.9 | Possible de-activation processes of electronically excited molecules (AB^*) in polar media | 54 |
| Figure 2.10 | Schematic Representation of the Magnetically Driven Transport of Drugs to a Specific Region | 64 |
| Figure 3.1 | A Simple Synthetic Apparatus Employed in the Preparation of Colloidal Nanoparticles | 68 |
| Figure 3.2 | Scheme of reaction for Ag Nanoparticles in PVP Stabilizing Medium with Glycerol as Reductant | 68 |
| Figure 3.3 | Scheme of Reaction for AgM Nanoparticles in PVP Stabilizing Medium with Glycerol as Reductant | 70 |
| Figure 3.4 | Scheme of Reaction for the Reduction of Metal ion in Liquid Phase | 72 |
| Figure 4.1 | Absorbance Spectra of (a) Ag SC; (b) Ag PET; (c) Ag HDA; (d) Ag GLY at 175°C | 78 |

| | | |
|-------------|---|----|
| Figure 4.2 | Absorbance Spectra of (e) Ag EG; (f) Ag GLY at 160 ⁰ C; (g) Ag TOPOOA and (h) Ag DEG | 79 |
| Figure 4.3 | PL Emission Spectra of (a) Ag GLY at 175 ⁰ C, 2h; (b) Ag DEG at 190 ⁰ C, 2h Excited at 315 nm | 80 |
| Figure 4.4 | PL Emission of (c) Ag TOPO/OA at 180 ⁰ C, 2h; (d) Ag HDA at 200 ⁰ C, 2h Excited at 340 nm | 81 |
| Figure 4.5 | TEM micrographs of Ag nanoparticles stabilized with (a) PVP/EG at 160 ⁰ C, 2h; (b) PVP/GLY at 160 ⁰ C, 2h; (c) HDA at 200 ⁰ C, 2h; (d) PVP/PET at 90 ⁰ C, 2h showing tunable morphology. | 83 |
| Figure 4.6 | (a) TEM Image of Ag NPs in PVP/EG at 160 ⁰ C, 2h showing its polycrystalline property; HRTEM Micrographs of Ag NPs stabilized with (b) PVP/GLY at 160 ⁰ C, 2h; showing agglomeration of spherical Ag NPs (c and d) PVP/SC at 90 ⁰ C, 2h showing clear lattice fringes | 84 |
| Figure 4.7 | XRD Patterns of Ag nanoparticles stabilized with (a) PVP/DEG; (b) HDA; (c) PVP/GLY; (d) PVP/EG; (e) PVP/PET and (f) PVP/SC | 86 |
| Figure 4.8 | UV-Vis Spectra of AgCo nanoparticles stabilized with PVP/GLY (a) 160 ⁰ C, 2h (b) at 175 ⁰ C, 2h (c) at 150 ⁰ C, 4h: PVP/EG (d) at 160 ⁰ C, 3h (e) at 175 ⁰ C, 2h | 87 |
| Figure 4.9 | UV-Vis Spectra of AgCo nanoparticles stabilized with PVP/DEG (a) at 200 ⁰ C, 2h and (b) at 190 ⁰ C, 2h | 88 |
| Figure 4.10 | Combined UV-Vis Absorption and PL emission of AgCo NPs | 89 |
| Figure 4.11 | PL Spectra of AgCo nanoparticles stabilized with PVP/GLY (a) at 150 ⁰ C, 4h (b) at 160 ⁰ C, 2h; (c) PVP/DEG at 190 ⁰ C, 2h; (d) PVP/EG at 160 ⁰ C, 3h | 89 |
| Figure 4.12 | TEM micrographs of AgCo Nanoparticles Stabilized with (a) PVP/GLY at 160 ⁰ C, 2h; (b) PVP/DEG at 190 ⁰ C, 2h; (c) PVP/EG at 175 ⁰ C, 2h; (d) HRTEM images of AgCo NPs Stabilized with PVP/DEG at 200 ⁰ C, 2h revealing the core-shell structure | 91 |
| Figure 4.13 | HRTEM images of AgCo NPs stabilized with (a, b and c) PVP/EG at 175 ⁰ C, 2h and (d) PVP/DEG at 200 ⁰ C, 2h, revealing the core-shell structure | 92 |
| Figure 4.14 | XRD Pattern of AgCo nanoparticles stabilized with PVP/GLY at 175 ⁰ C, 2h | 93 |

| | | |
|-------------|---|-----|
| Figure 4.15 | (a) XPS Spectrum of AgCo Nanoparticles Stabilized with PVP/DEG at 200°C, 2h | 94 |
| Figure 4.15 | (b) High Resolution Scan of Ag 3d Core levels of AgCo Nanoparticles Stabilized with PVP/DEG at 200°C, 2h | 95 |
| Figure 4.16 | (a) XPS High Resolution Scan with the Deconvolution for the O (1s) core levels | 95 |
| Figure 4.16 | (b) XPS High Resolution Scan with the Deconvolution for the Co (2p) core levels | 96 |
| Figure 4.17 | UV-Vis Spectra of AgNi NPs stabilized with (a) PVP/DEG at 190°C, 2h (b) PVP/GLY at 160°C, 2h (c) PVP/EG at 175°C, 2h | 97 |
| Figure 4.18 | UV-Vis Spectra of AgNi NPs stabilized with PVP/EG (a) at 175°C, 2h and (b) at 160°C, 3h | 98 |
| Figure 4.19 | PL Spectra of AgNi NPs stabilized with (a) PVP/EG at 175°C, 2h (blue); 160°C, 3h (red) (b) AgNi NPs stabilized with PVP/GLY at 160°C, 2h (red) and 150°C, 4h (blue) | 99 |
| Figure 4.20 | (a and b) TEM images of AgNi NPs stabilized with PVP/GLY at 160°C, 2h; (c and d) corresponding HRTEM images of (a and b) | 101 |
| Figure 4.21 | TEM images of AgNi NPs stabilized with (a) PVP/DEG at 200°C, 2h, (b) PVP/EG at 160°C, 3h, (c and d) corresponding HRTEM images of (a and b) | 102 |
| Figure 4.22 | XRD Patterns of AgNi nanoparticles stabilized with (a) PVP/DEG at 190°C, 2h; (b) PVP/GLY at 160°C, 2h; (c) PVP/EG at 160°C, 3h | 104 |
| Figure 4.23 | (a) XPS Spectrum of AgNi nanoparticles stabilized with PVP/DEG at 200°C, 2h | 105 |
| Figure 4.23 | (b) High Resolution Scan of Ag (3d) core levels of AgNi nanoparticles stabilized with PVP/DEG at 200°C, 2h | 106 |
| Figure 4.24 | (a) High Resolution Scan of Ni (2p) core levels | 106 |
| Figure 4.24 | (b) High Resolution Scan O (1s) core levels | 107 |
| Figure 4.25 | Absorption spectra of AgPd NPs stabilized with (a) PVP/GLY at 160°C, 2h; (b) PVP/DEG at 190°C, 2h; (c) PVP/EG, 175°C, 2h; (d) PVP/DEG at 200°C, 2h; (e) PVP/EG at 160°C, 3h | 108 |
| Figure 4.26 | Mechanism of Ag-Pd bimetallic nanoparticles by the successive reduction of Pd and Ag ions with polyol in the presence of PVP | 110 |

| | | |
|-------------|--|-----|
| Figure 4.27 | (a) PL Spectra of AgPd NPs stabilized with (a) PVP/EG, 160 ⁰ C, 3h (red for an excitation at 325 nm; brown: 232 nm) | 111 |
| Figure 4.27 | (b) PVP/DEG, 190 ⁰ C, 2h; PVP/EG, 160 ⁰ C, 3h; PVP/GLY 175 ⁰ C, 2h | 111 |
| Figure 4.27 | (c) Combined UV-Visible and PL spectra of AgPd sol PVP/DEG at 190 ⁰ C, 2h, absorption wavelength: 383 nm; PL emission at 346 nm for an excitation at 315 nm | 112 |
| Figure 4.28 | TEM images of AgPd NPs stabilized with (a) PVP/DEG at 200 ⁰ C, 2h; (b) PVP/EG, 160 ⁰ C, 3h; (c and d) HRTEM images of (a and b) respectively | 113 |
| Figure 4.29 | (a) TEM image of AgPd NPs stabilized with PVP/GLY at 160 ⁰ C, 2h; HRTEM images of AgPd NPs stabilized with (b) PVP/EG at 160 ⁰ C, 3h; (c, d) PVP/GLY at 160 ⁰ C, 2h showing high index faceted nanostructures | 114 |
| Figure 4.30 | XRD Pattern showing the polycrystalline nature of Ag/Pd nanoparticles stabilized with (a) PVP/GLY at 160 ⁰ C, 2h and (b) PVP/EG at 160 ⁰ C, 3h and (c) PVP/DEG at 200 ⁰ C, 2h | 115 |
| Figure 4.31 | (a) XPS Spectrum of High Resolution Scan of AgPd Nanoparticles Stabilized with PVP/DEG at 200 ⁰ C, 2h | 117 |
| Figure 4.31 | (b) High Resolution Scan of Ag (3d) of Core Levels of AgPd Nanoparticles Stabilized with PVP/DEG at 200 ⁰ C, 2h | 117 |
| Figure 4.32 | (a) High Resolution Scan of Pd (3d) core levels | 118 |
| Figure 4.32 | (b) High Resolution Scan of O (1s) core levels | 118 |
| Figure 4.33 | (a) UV-Vis Spectra of AgPt NPs stabilized with (a) PVP/DEG at 190 ⁰ C, 2h (blue); PVP/EG at 160 ⁰ C, 3h (red); PVP/GLY at 160 ⁰ C, 2h (green) | 119 |
| Figure 4.33 | (b) Absorption spectra of AgPt NPs stabilized PVP/GLY at 175 ⁰ C, 2h for 2:1 and 3:1 of Ag and Pt precursors | 120 |
| Figure 4.34 | (a) PL emission spectra of AgPt sols showing the effect of different stabilizers | 122 |
| Figure 4.34 | (b) PL emission spectra of AgPt sols stabilized with PVP/EG at 160 ⁰ C, 3h for excitation at dual wavelengths | 122 |
| Figure 4.34 | (c) PL emission spectra of AgPt sol stabilized with PVP/GLY at 160 ⁰ C, 2h showing the effect of change in temperature | 123 |

| | | |
|-------------|---|-----|
| Figure 4.34 | (d) Combined UV-Visible and PL emission spectra of AgPt GLY at 160°C, 2h, absorption maximum at 388 nm, PL emission at 348 nm for an excitation at 245 nm | 123 |
| Figure 4.35 | TEM images of AgPt NPs stabilized with: (a) PVP/DEG at 200°C, 2h (b) PVP/EG at 160°C, 3h (c) PVP/GLY at 165°C, 4h and (d) PVP/GLY at 160°C, 2h | 125 |
| Figure 4.36 | HRTEM images (a, b and inset c) AgPt NPs stabilized with PVP/GLY at 160°C, 2h; (d, e) AgPt NPs stabilized with PVP/EG at 160°C, 3h | 126 |
| Figure 4.37 | (a, b) HRTEM images of AgPt NPs stabilized with PVP/DEG at 200°C, 2h | 127 |
| Figure 4.38 | XRD Patterns showing the polycrystalline nature of Ag/Pt nanoparticles stabilized with (a) PVP/GLY at 160°C, 2h and (b) PVP/DEG at 200°C, 2h and (c) PVP/EG at 160°C, 3h | 129 |
| Figure 4.39 | (a) XPS Spectrum of high resolution scan of AgPt nanoparticles stabilized with PVP/DEG at 200°C, 2h | 130 |
| Figure 4.39 | (b) High resolution scan of Ag (3d) core levels of AgPt nanoparticles stabilized with PVP/DEG at 200°C, 2h | 131 |
| Figure 4.40 | (a) High Resolution Scan of Pt (4f) core levels | 131 |
| Figure 4.40 | (b) High Resolution Scan of O (1s) core levels | 132 |
| Figure 4.41 | UV-Visible Spectra of AgRu sols stabilized with DT in the presence of (a) glycerol (b) diethylene glycol and (c) ethylene glycol at 200°C, 3h; (d) Ru sol stabilized with DT in the presence ethylene glycol at 200°C, 3h | 133 |
| Figure 4.42 | (a) Combined UV-Visible Absorbance/Photoluminescence emission Spectra of AgRu DEG/DT at 200°C, 3h: maximum absorbance at 388 nm; multiphoton PL emission at 334, 408 and 645 nm for an excitation at 300 nm | 135 |
| Figure 4.42 | (b) Combined UV-Visible Absorption/Photoluminescence emission Spectra of AgRu EG/DT at 200°C, 3h: maximum absorbance at 387 nm; multiphoton PL emission at 343, 396 and 662 nm for an excitation at 315 nm | 135 |

| | | |
|-------------|--|-----|
| Figure 4.42 | (c) Combined UV-Visible Absorption/Photoluminescence emission Spectra of AgRu GLY/DT at 200 ⁰ C, 3h: maximum absorbance at 387 nm; multiphoton PL emission at 335, 402 and 646 nm for an excitation at 300 nm | 136 |
| Figure 4.43 | TEM images (a-b) AgRu NPs stabilized with DT/EG at 200 ⁰ C, 3h showing the polydispersed nature of the nanocomposite; (c, d) AgRu NPs stabilized with DT/GLY at 200 ⁰ C, 3h revealing a nearly monodispersed and well-ordered crystalline structure | 137 |
| Figure 4.44 | HRTEM images of AgRu NPs stabilized with (a) DT/EG and (b) DT/GLY at 200 ⁰ C, 3h (c) TEM image of AgRu NPs stabilized with DT/DEG at 200 ⁰ C, 3h and (d) its corresponding HRTEM image clearly showing formation of alloy structure with lattice fringes | 138 |
| Figure 4.45 | XRD Pattern showing the polycrystalline nature of Ag/Ru nanoparticles stabilized with DT/DEG; DT/EG; DT/GLY at 200 ⁰ C, 3h | 140 |
| Figure 4.46 | UV-Visible Spectra of (a) AgRu (b) AgCo (c) AgNi (d) AgPt and (e) AgPd sols stabilized with PVP/PET at 90 ⁰ C, 4h | 141 |
| Figure 4.47 | UV-Visible spectra of (a) AgPd (b) Ag (c) AgNi (d) AgPt and (e) AgCo sols stabilized with PVP/SC at 90 ⁰ C, 2h | 142 |
| Figure 4.48 | (a) Combined UV-Visible/PL Emission Spectra of AgPt PET at 90 ⁰ C, 4h: maximum absorbance at 236 nm; PL emission at 390 nm for an excitation at 335 nm | 144 |
| Figure 4.48 | (b) Combined UV-Visible/PL Emission Spectra of AgCo PET at 90 ⁰ C, 4h: maximum absorbance at 416 nm; PL emission at 390 nm for an excitation at 340 nm | 145 |
| Figure 4.48 | (c) Combined UV-Visible/PL Emission Spectra of AgNi PET at 90 ⁰ C, 4h: maximum absorbance at 422 nm; PL emission at 386 nm for an excitation at 340 nm | 145 |
| Figure 4.49 | TEM images (a) AgNi NPs; (b) AgPd NPs functionalized with PVP/PET at 90 ⁰ C, 4h | 146 |
| Figure 4.50 | (a, b) TEM images of AgRu NPs; HRTEM images (c) AgCo NPs; (inset d) core-shell morphology of (c); (e) AgNi NPs functionalized with PVP/PET at 90 ⁰ C, 4h | 147 |

| | | |
|-------------|--|-----|
| Figure 4.51 | HRTEM images (a) AgPd NPs; inset (b) showing the core-shell nanosphere of (a); (c) AgRu NPs; (d, e) AgPt NPs functionalized with PVP/PET at 90 ⁰ C, 4h | 148 |
| Figure 4.52 | HRTEM images (a, b) AgCo NPs; (c, d) AgPd NPs capped with PVP/SC at 90 ⁰ C, 2h | 150 |
| Figure 4.53 | XRD Patterns of (a) AgPd NPs, (b) AgRu NPs and (c) AgPt core-shell NPs functionalized with PVP/PET at 90 ⁰ C, 4h; (d) AgPd NPs and (e) AgNi NPs capped with PVP/SC at 90 ⁰ C, 2h | 152 |
| Figure 4.54 | (a) XPS Spectrum of High Resolution Scan of AgRu nanoparticles stabilized with PVP/PET at 90 ⁰ C, 4h | 154 |
| Figure 4.54 | (b) High Resolution Scan of Ag (3d) core levels of AgRu nanoparticles stabilized with PVP/PET at 90 ⁰ C, 4h | 154 |
| Figure 4.55 | (a) XPS Spectrum of High Resolution Scan of O (1s) core levels | 155 |
| Figure 4.55 | (b) High Resolution Scan of Ru (3d) core levels | 155 |
| Figure 4.56 | (a) UV-Visible Spectra of Ag and Ag allied bimetallic sols capped with HDA at 200 ⁰ C, 2h | 156 |
| Figure 4.56 | (b) UV-Visible Spectra of Ag allied bimetallic sols capped with TOPO/OA at 180 ⁰ C, 2h | 157 |
| Figure 4.57 | (a) Combined UV-Visible/PL emission Spectra of AgCo capped with HDA at 200 ⁰ C, 2h, maximum absorbance at 409 nm, PL emission at 373 and 461 nm for an excitation at 340 nm | 159 |
| Figure 4.57 | (b) Combined UV-Visible/PL emission Spectra of AgNi HDA at 200 ⁰ C, 2h, maximum absorbance at 415 nm, PL emission at 378 nm for an excitation at 340 nm | 159 |
| Figure 4.57 | (c) Combined UV-Visible/PL emission Spectra of AgPt HDA at 200 ⁰ C, 2h, maximum absorbance at 346 nm, PL emission at 396 nm for an excitation at 340 nm | 160 |
| Figure 4.57 | (d) Combined UV-Visible/PL emission Spectra of AgPt TOPO/OA at 180 ⁰ C, 2h, maximum absorbance at 274 nm; PL emission due to S ₁ - S ₀ transition at 391 nm for an excitation at 340 nm | 160 |
| Figure 4.58 | TEM images (a) AgCo NPs; (b) AgNi NPs; (c, d) HRTEM images of a, b respectively; inset (e) core-shell structure of (c) capped with TOPOOA at 180 ⁰ C, 2h | 162 |

| | | |
|-------------|--|-----|
| Figure 4.59 | (a) TEM image of AgPd NPs; HRTEM images (b) AgPd NPs; (c, d) AgPt NPs capped with TOPOOA at 180 ⁰ C, 2h; (e) TEM image of AgRu NPs capped with TOPOOA at 180 ⁰ C, 3h | 163 |
| Figure 4.60 | (a, b) HRTEM images of AgCo NPs; (c, d) TEM/HRTEM images of AgNi NPs respectively, capped with HDA at 200 ⁰ C, 2h | 165 |
| Figure 4.61 | (a, b) TEM images of AgPd and AgPt NPs respectively; (c, d) HRTEM images of AgPd and AgPt NPs respectively; inset (e) HRTEM image of (d) capped with HDA at 200 ⁰ C, 2h | 166 |
| Figure 4.62 | 4.62: XRD patterns of (a) TOPOOA capped AgRu nanoparticles at 180 ⁰ C, 3h; HDA capped (b) AgPd NPs; (c) AgCo NPs; (d) AgNi NPs at 200 ⁰ C, 2h | 168 |
| Figure 4.63 | (a) XPS High Resolution Surface Scan of AgRu nanoparticles capped with TOPOOA at 180 ⁰ C, 3h | 169 |
| Figure 4.63 | (b) Ag (3d) core level high resolution deconvolution scan of AgRu nanoparticles capped with TOPOOA at 180 ⁰ C, 3h | 170 |
| Figure 4.64 | (a) XPS High Resolution Surface Scan of Ru (3d) core levels | 170 |
| Figure 4.64 | (b) XPS High Resolution deconvolution Scan of O (1s) core levels | 171 |
| Figure 4.65 | Formation mechanism of M ₁ -core/M ₂ -shell structured bimetallic nanoparticles | 172 |
| Figure 4.66 | Proposed formation process of PVP-protected AgPt bimetallic Nanoparticles | 173 |
| Figure 4.67 | TEM images (a, b) Co NPs; (c) Ni NPs stabilized with EG at 190 ⁰ C, 4h; (d) HRTEM image of (c) | 174 |
| Figure 4.68 | TEM images (a) Pd NPs; (b, c) Pt NPs stabilized with PVP/GLY at 160 ⁰ C, 2h. HRTEM images (d) Pd NPs; (e) Pt NPs passivated with PVP/SC at 90 ⁰ C, 2h | 175 |
| Figure 4.69 | TEM images (a) Co NPs stabilized with PVP/PET at 90 ⁰ C, 2h, (b) Ru NPs stabilized with DT/EG at 200 ⁰ C, 3h and (c) HRTEM image of (b) | 176 |
| Figure 4.70 | XRD Patterns of (a) Ni NPs stabilized with PVP/N ₂ H ₄ at 90 ⁰ C, 2h; (b) Pd NPs (c) Pt NPs stabilized with PVP/GLY at 160 ⁰ C, 2h | 177 |

| | | |
|-------------|---|-----|
| Figure 4.71 | (a) Change in Absorbance at 400 nm as a Function of Time Using Ag Allied Nanobimetallic Particles Prepared as Catalysts::AgPt in PVP/EG at 170 ⁰ C, 4h | 180 |
| Figure 4.71 | (b) Change in Absorbance at 400 nm as a Function of Time Using Ag Allied Nanobimetallic Particles Prepared as Catalysts: AgPt in PVP/GLY at 165 ⁰ C, 4h | 181 |
| Figure 4.72 | Plots of $\ln (A/A_0)$ (A: absorbance at fixed intervals, A_0 : absorbance at time, t close to infinity) and the reaction time, t (s) at 299 K for (a, b) AgPd PVP/GLY, 160 ⁰ C, 2h | 185 |
| Figure 4.73 | (a) Plots of $\ln (A/A_0)$ (A: absorbance at fixed intervals, A_0 : absorbance at time, t close to infinity) and the reaction time, t (s) at 299 K; (b) plot of observed rate constant, K^1 vs amount of $[BH_4^-]$ consumed by AgPd PVP/GLY, 160 ⁰ C, 2h reduction of 4NP | 186 |
| Figure 4.74 | Plots of $\ln (A/A_0)$ (A: absorbance at fixed intervals, A_0 : absorbance at time, t close to infinity) and the reaction time, t (s) at 299 K for (a) AgPt PVP/GLY, 175 ⁰ C, 2h ; (b) AgPt PVP/SC, 90 ⁰ C, 2h | 187 |
| Figure 4.75 | Plots of $\ln (A/A_0)$ (A: absorbance at fixed intervals, A_0 : absorbance at time, t close to infinity) and the reaction time, t (s) at 299 K for (a) AgPd PVP/EG, 170 ⁰ C, 4h; (b) AgPt PVP/SC(2), 90 ⁰ C, 2h | 188 |
| Figure 4.76 | Plots of $\ln (A/A_0)$ (A: absorbance at fixed intervals, A_0 : absorbance at time, t close to infinity) and the reaction time, t (s) at 299 K for (a) AgPd PVP/PET, 90 ⁰ , 4h ; (b) AgPt PVP/GLY, 165 ⁰ C, 4h | 189 |
| Figure 4.77 | Plots of $\ln (A/A_0)$ (A: absorbance at fixed intervals, A_0 : absorbance at time, t close to infinity) and the reaction time, t (s) at 299 K for (a) AgPt PVP/EG, 170 ⁰ C, 4h; (b) AgPt PVP/DEG, 195 ⁰ C, 4h | 190 |
| Figure 4.78 | Plots of $\ln (A/A_0)$ (A: absorbance at fixed intervals, A_0 : absorbance at time, t close to infinity) and the reaction time, t (s) at 299 K for (a) AgPt PVP/PET, 90 ⁰ C, 4h; (b) AgPd PVP/DEG, 190 ⁰ C, 4h | 191 |
| Figure 4.79 | Plots of $\ln (A/A_0)$ (A: absorbance at fixed intervals, A_0 : absorbance at time, t close to infinity) and the reaction time, t (s) at 299 K for AgPd PVP/GLY, 170 ⁰ C, 4h | 192 |

LIST OF ACRONYMS AND ABBREVIATIONS

| | |
|--------|--|
| EG | Ethylene glycol |
| DEG | Diethylene glycol |
| GLY | Glycerol |
| PET | Pentaerythritol |
| HDA | Hexadecylamine |
| TOPO | Trioctylphosphine oxide |
| DT | Dodecanethiol |
| DOE | Dioctyl ether |
| OA | Oleic acid |
| PVP | Polyvinylpyrrolidone |
| TEM | Transmission electron microscope |
| HRTEM | High resolution transmission electron microscope |
| XRD | X-ray diffractometer |
| p-XRD | Powder x-ray diffraction |
| EDX | Energy dispersive x-ray microanalyzer |
| XPS | X-ray photoelectron spectrometer |
| AES | Auger electron spectroscopy |
| UV-Vis | Ultraviolet-Visible |
| PL | Photoluminescence |
| PLE | Photoluminescence excitation |
| SC | Trisodium citrate trihydrate |
| NPs | Nanoparticles |
| BNPs | Bimetallic nanoparticles |
| 4-NP | 4-nitrophenol |
| p-NP | para-nitrophenol |
| fcc | Face centered cubic |
| hcp | Hexagonal close packed |
| 1D | One dimension |
| 2D | Two dimensions |
| 3D | Three dimensions |
| EXAFS | Extended X-ray absorption fine structure |
| SPR | Surface plasmon resonance |

| | |
|-------|--|
| SRB | Surface resonance band |
| CVD | Chemical vapour deposition |
| PVD | Physical vapour deposition |
| MBE | Molecular beam epitaxy |
| MOCVD | Metallorganic chemical vapour deposition |
| STP | Standard temperature and pressure |
| CTAB | Cetyltrimethylammonium bromide |
| SDS | Sodium dodecyl sulphate |
| AOT | Diocetyl sulfosuccinate sodium salt |
| IR | Infra-red |
| FWHM | Full width at half maximum |
| LO | Lattice Oxygen |
| eV | Electron volt |
| nm | Nanometer |
| Å | Angstrom |
| °C | Degree Celsius |
| K | Kelvin |
| aq | Aqueous |

ABSTRACT

The synthesis of seed mediated AgM (M = Co, Ni, Ru, Pd and Pt) allied nanobimetallic particles was successfully carried out by simultaneous reduction in aqueous and non-aqueous solutions. The formation of novel monodispersed and unaggregated bimetallic nanoparticles capped by polymer and organic chelating agents was desirable for catalysis and photonic applications. As a result, wet chemical approach was successfully deployed to produce some novel bimetallic silver allied nanoparticles distinct in morphology from their monometal analogues. Optical and morphological investigation of the nanoparticles revealed that the shape, size and size distribution of the silver allied nanoparticles depended on the stabilizer or capping agent, mole ratio of inorganic sources, temperature and time of reaction. The analyses of the nanoparticles also showed that formation of uniformly distributed, highly crystalline and monodispersed/polydispersed silver allied bimetallic nanocomposites of different dimensions within the quantum realm had been achieved. Consequently, the alloy or core-shell crystalline structure of nanocomposites was also established. Furthermore, X-ray photoelectron spectrometer (XPS) scan established the surface elemental composition and the binding energy of the nanocomposites. As a result, a new morphology described as hybrid quasi nanocubes entangled in nanowebs was discovered for polyvinylpyrrolidone (PVP) stabilized AgPt nanoparticles passivated by diethylene glycol (DEG) and ethylene glycol (EG) which evolved a core-shell structure. The mean size of the nanocubes was 30.45 ± 6.23 nm, while XRD analysis strongly suggested that the nanocubes pertained to {111} plane of face-centered cubic Ag. Meanwhile, the nanoweb was formed as a result of phase contraction by Pt. Likewise, electron micrographs of Ag/Ru nanoparticles capped by dodecanethiol/polyol at 200°C; 3h showed the presence of novel well-ordered core-shell structures with particle size in the range of 8.2 ± 0.7 - 11.4 ± 1.3 nm. In addition, novel core-shell nanoparticles of AgPt capped by hexadecylamine (HDA) were discovered from their electron micrographs. The X-ray diffraction spectra suggested dominance of face-centered cubic structure with 2θ reflections slightly shifted from silver peaks. This is reminiscent of noble metals forming alloy or core-shell morphology with silver. Similarly, AgCo and AgNi nanoparticles passivated by polyol particularly revealed the formation of nearly uniform, monodispersed core-shell structure which proved to be optically active by characteristic surface plasmon resonance band blue shifted for pentaerythritol (PET) and trisodium citrate trihydrate (SC) derived nanoparticles. Further optical characterization also revealed the fluorescent potential of AgCo, AgNi, AgPt, AgPd and AgRu sols as a result of their S_1 - S_0

vibrational mode relaxation with appreciable emission of appropriate quantum yield. Finally, the catalytic potential of the nanocomposites investigated using 4-nitrophenol in the presence of sodium borohydride at 299 K indicated a pseudo-first-order kinetics which gave AgPd/PVP_{GLY} a rate constant of $5.4 \times 10^{-3} \text{ s}^{-1}$. This value is significantly higher than $2.8 \times 10^{-3} \text{ s}^{-1}$ reported for poly(ethylenimine)-stabilized Ag nanoparticles (Ag-HNP), but relatively lower than $9.2 \pm 1.7 \times 10^{-3} \text{ s}^{-1}$ recorded for AuAg-HNP due to the fact that Au/Ag bimetallic nanoparticles have been shown to exhibit greater quantum size effect. These results strongly indicate the application of these materials for catalysis and optoelectronics.